ELSEVIER

Polymer 41 (2000) 2999–3010

polymer

Comparative study of the crystalline morphology present in isotropic and uniaxially stretched "conventional" and metallocene polyethylenes

J.M. Lagarón[a,*], S. López-Quintana[b], J.C. Rodriguez-Cabello[a], J.C. Merino[a], J.M. Pastor[a]

[a]*Física de la Materia Condensada, E.T.S.I.I., University of Valladolid, 47011 Valladolid, Spain*
[b]*CIDAUT, Technological Park of Boecillo, 47151 Valladolid, Spain*

Received 7 April 1999; accepted 24 June 1999

Abstract

A comparative study of the crystalline phase present in conventional and metallocene polyethylenes covering a broad range in density (953–885 kg/m^3) has been carried out using Raman, DSC and WAXS. The materials were compared in the isotropic state, after uniaxial stretching at room temperature, and after annealing of the stretched material. Crystallinity for the isotropic samples and relative molecular orientation for the stretched samples decreased with decreasing density. The Raman crystallinity (using Strobl–Hagedorn's approach) was found to decrease more rapidly with density than crystallinity by the other techniques. Upon cold drawing, the three techniques supported a disruption of the crystalline morphology towards a highly ill-defined and fractured orthorhombic crystalline phase. The disruption of the crystallinity was more dramatic for the lower densities most likely due to branched molecules being pulled through the crystals. The perfection of the orthorhombic crystallinity was further restored upon annealing. Changes in the position of the two components of the $-CH_2-$ bending factor group splitting, i.e. the crystallinity band at 1415 cm^{-1} and the band at 1440 cm^{-1}, were measured as a function of sample density and physical treatment and were attributed to alterations in crystalline density and perfection. Particular behaviours observed for the materials were attributed to their particular molecular architecture.

Keywords: Polyethylene; Raman spectroscopy; Cold drawn material

1. Introduction

The understanding of the structure–properties relationship of ethylene-based polymers has been one of the main topics of fundamental research over the last decades. During this time span, the development of these commodity materials has been continuous in order to overcome the successive challenges imposed by the market and the advent of new competitive products, as well as to improve and diversify overall performance. New technologies in polymerisation processes and catalysts have broadened considerably the range of materials available. The discovery and posterior development of low density (LDPE) and high-density (HDPE) polyethylenes was followed by lineal (LLDPE) and bimodal polyethylenes. More recently (in the 1990s), a new range of polyethylene grades with a highly regular molecular design has been attained by means of single site metallocene-based catalysts [1] and vanadium-based catalysts [2]. These materials are usually called homogeneous polyethylenes because they display a highly homogeneous molecular structure with narrow molecular weight distribution and a random incorporation of the comonomer inter- and intra-molecularly. Conversely, heterogeneous polyethylenes, i.e. LLDPEs and bimodal materials, display a broader molecular weight distribution and heterogeneous incorporation (inter- and/or intra-molecularly) of the comonomer over the molecular weight [3]. The improvement in the control over the molecular design achieved by this new generation of catalysts provides the researchers with a new range of materials to extend the characterisation of this family of polymers.

The microstructure of the homogeneous copolymers obtained by the Dow's INSITE™ constrained geometry catalyst technology (based on metallocene chemistry) has been recently classified as a function of sample density using transmission electron microscopy (TEM) and others techniques [1]. The suggested morphologies go from lamellaes superstructured into spherulites for the highest densities (HDPE-like) to bundle-like fringed micellar crystals for the lowest densities (<890 kg/m^3) with elastomeric-like behaviour. Intermediate densities show a mixture of both

* Corresponding author. BP Chemicals, Applied Technology 7, P.O. Box 21, Grangemouth FK3 9XH, UK.

0032-3861/00/$ - see front matter
PII: S0032-3861(99)00459-0

Table 1
Sample characteristics, melting point (maximum of melting) and the annealing temperatures of the materials used

Nomenclature	HDPE	LDPE	LLDPE (Dowlex)	POP (Affinity)	POE (Engage)
Density (kg/m^3)	953	923	918	903	885
[a]Melt index (g/10 min)	4.0	3.5	2.3	1.0	1.0
M_w	79 800	68 000	82 000	80 800	90 600
M_w/M_n	3.3	3.3	3.4	2.2	2.0
Melting point (°C)	130	111	125	101	82
Annealing temperature (°C)	105	88	100	80	64

[a] 190°C, 2.16 kg

morphologies. In a paper by Mathod et al. [2] it is shown that vanadium-based catalysts can yield similar homogeneous polyethylene's.

A previous study [4] using Raman spectroscopy and other techniques, and dealing with the characterisation of uniaxially stretched (cold drawn) HDPE materials, showed that a decrease in the Raman crystallinity (ca. 30%) and a shift in position ($+1$ cm^{-1}) of the crystallinity band occurs upon cold drawing. The Raman crystallinity band is thought to arise from interchain interaction within the orthorhombic unit cell called factor group splitting. The decrease in the Raman orthorhombic crystallinity was attributed to the creation of a highly disrupted and defective orthorhombic crystalline morphology with some phase transformation to monoclinic phase (characterised by wide angle X-ray scattering (WAXS)) and possibly, some chain unfolding. The disruption of some of the orthorhombic crystals occurred to such an extent that no longer results in effective interchain interaction, i.e. in factor group splitting, is thought to cause this drop in the Raman crystallinity. The shift in position towards a higher wavenumber observed for the crystallinity band was associated with a decrease in the interchain interaction efficiency within the lattice, and therefore to lateral disorder. Crystallinity by DSC though, measured no difference between isotropic and cold drawn materials. The annealing of the stretched structure restored the Raman orthorhombic crystalline phase towards the perfectness of the isotropic undeformed crystals and left virtually unchanged the high molecular orientation of the stretched specimens. The study concluded that uniaxial deformation at room temperature and below of HDPE fractures and subsequently extends the crystalline lamellae due to molecules being pulled through the crystals. The latter effect results at the molecular scale in a dramatic loss of the chain lateral order in the orthorhombic lattice, to which the Raman crystallinity band is highly sensitive. A recent study [5] carried out on a varied range of polyethylenes, reported a significant increase in all-trans chain segments with decreasing density upon uniaxial stretching. The increase of the all-trans segments within the chains was attributed to orientation in the amorphous regions and in particular to stress-induced orientation of tie-molecules and other topological constrains trapped between crystals.

In the work reported here, we carry out a comparative characterisation of the crystalline structure of a group of PEs covering a broad range of density and molecular designs. The polymers were subjected to uniaxial deformation and annealing and were studied by Raman spectroscopy, DSC and WAXS. We aim to assess all the structural features cited above and get more insight into the Raman analysis of the polyethylene crystallinity as a function of density by comparison with DSC and WAXS data.

2. Experimental

2.1. Samples

Five different polyethylene grades (kindly supplied by Dow Iberica, Spain) were used in this study. Some sample characteristics are summarised in Table 1. All materials except LDPE are ethylene-1-octene copolymers. The content of the comonomer increases with decreasing density although the actual numbers were not supplied. Samples were selected to match, as close as possible, molecular weight. Consequently, differences in behaviour can be mainly attributed to differences in molecular architecture arising from the incorporation of the comonomer. The samples POP and POE were obtained using the so-called Insite™ (metallocene-based) technology [1].

Dumb-bell specimens were die-stamped from 2 mm thick compression moulded plates. The polymer plates were obtained by holding pellet material at ca. 50°C above the maximum of melting for five minutes and then cooled under pressure at 20°C/min in a hot plate press. The dumb-bells gauche length shape was semicircular (10 mm diameter) in order to ensure a continuous increasing stress for the material during the stretching process. Uniaxial stretching at room temperature (cold drawing) was carried out in a computer controlled stretching rig (Minimat, Polymer Laboratories) at a constant speed of 10 mm/min. The experiment was stopped when the neck reached two marks equally separated for all materials. Sample drawability decreased with decreasing sample density. The experiments described in this study were carried out on the stressless (free-ends) samples. In these stretched specimens, the Raman, WAXS and DSC experiments were carried out in material taken

Table 2
Crytallinity (%) by DSC of isotropic, stretched and annealed stretched materials. The temperature (°C) range used for the integration of the heat of fusion is also provided

Sample	Isotropic	Stretched	Annealed stretched
HDPE	67 (30–150)	68 (31–152)	72 (35–152)
LDPE	46 (10–137)	47 (10–138)	49 (10–138)
LLDPE	42 (11–138)	45 (11–139)	45 (11–139)
POP	33 (17–118)	34 (17–119)	32 (17–119)
POE	24 (5–110)	26 (5–110)	23 (8–111)

from the middle of the dumb-bell. There the deformation is expected to be higher.

The annealing of isotropic and stretched samples was carried out in an oven for 1 h at temperatures ca. 20°C below the maximum of melting in the DSC thermograms of the isotropic samples. The stretched samples underwent significant shrinkage as a consequence of the annealing process, except the HDPE. The annealing temperatures are displayed in Table 1.

2.2. DSC

DSC measurements were carried out in a Mettler (Greinfensee, Switzerland) TA 4000 thermal analysis equipment The sample weight was ca. 3.5 mg and the heating rate was 10°C/min. Calibration of temperature and melting enthalpy was performed with an indium sample. The degree of crystallinity was calculated using the following equation:

$$\%\chi\text{-DSC} = \left(\frac{\Delta H_{\text{exp}}}{\Delta H^{\circ}}\right)100 \quad (1)$$

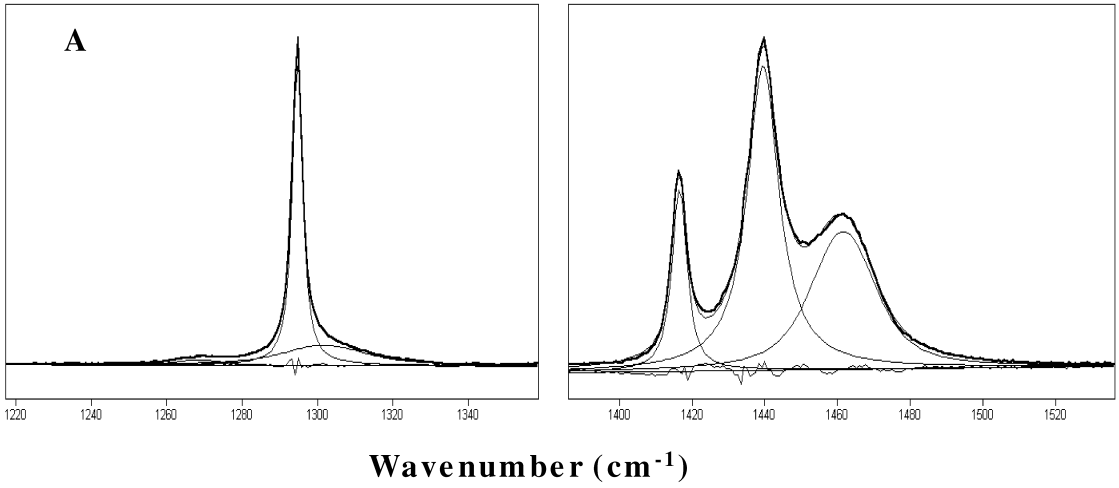

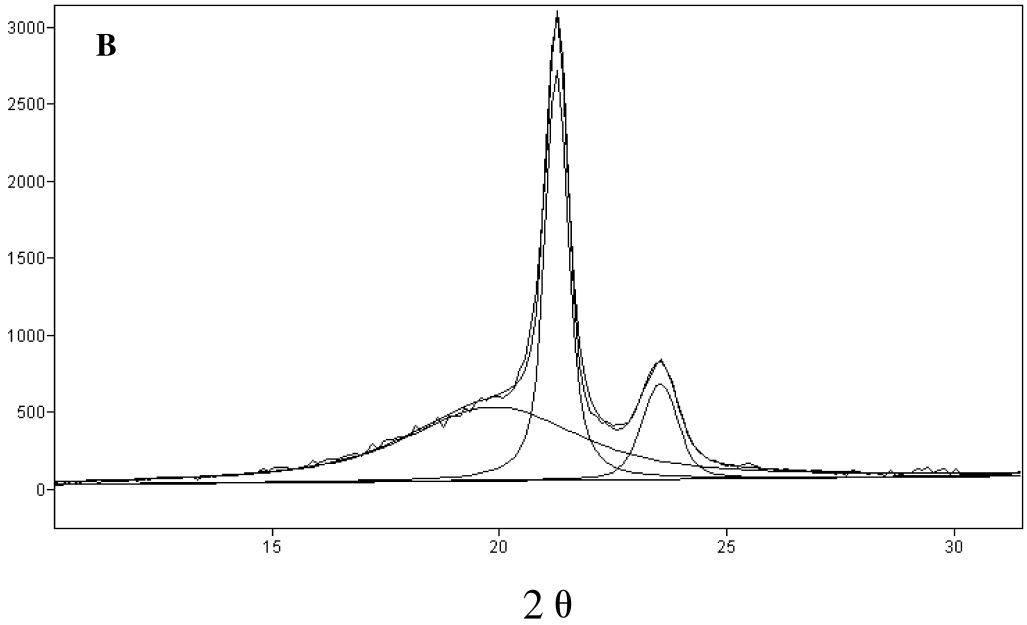

Fig. 1. Example of curve fitting of (A) Raman and (B) WAXS data for sample HDPE.

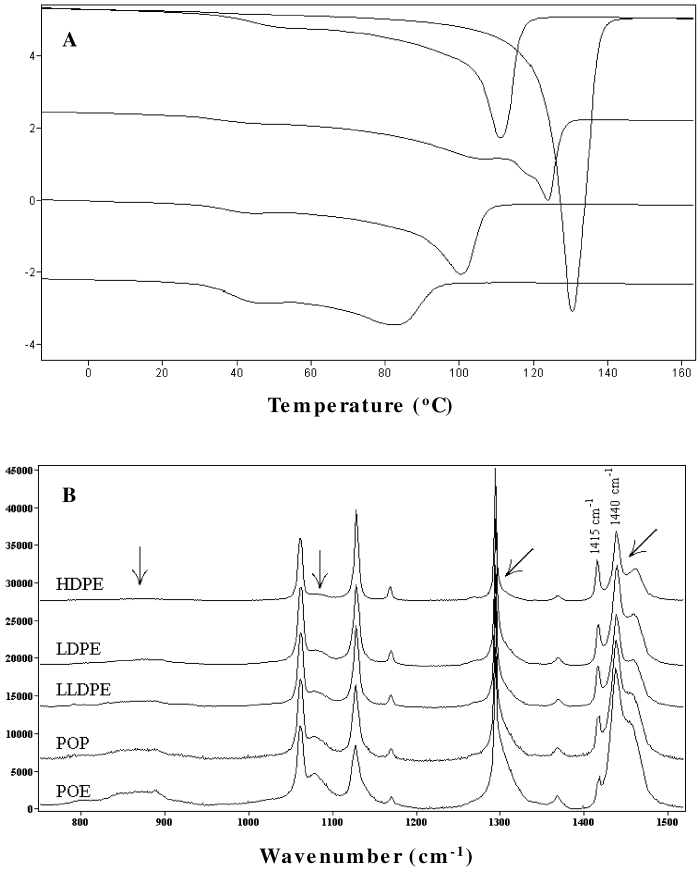

Fig. 2. (A) DSC melting endotherms and (B) Raman spectra of, from top to bottom, HDPE, LDPE, LLDPE, POP, POE.

where ΔH_{exp} is the experimentally determined heat of fusion and $\Delta H°$ is the heat of fusion for an infinitum polyethylene crystal at 290 J g^{-1}. The range of temperature used for the integration of the heat of fusion is summarised in Table 2 for each sample.

2.3. Raman spectroscopy

The "LabRam" micro-Ramam equipment of Dilor (France, SA) was used to record the Raman spectra. This equipment uses a 632 nm excitation source (HeNe laser), which results in typically 16 mW at the sample. Other experimental conditions of the set up were: 500 μm pinhole, 50× objective and 1800 grooves/mm diffraction gratings. Raman polarisation measurements were carried out on the samples by polarising the incident laser beam and analysing the scattered light parallel to the sample straining direction in the case of the stretched samples. This is denominated throughout the paper as polarisation $^1I_1$.

The Raman crystallinity for the isotropic samples was calculated using the method devised by Strobl and Hagedorn [6] (see Eq. (2)).

$$\%\chi\text{-Raman} = \left(\frac{I_{1415}}{0.45 \cdot I_{1300}}\right)100 \quad (2)$$

where I_{1415} is the integrated area of the 1415 cm^{-1} Raman band (the crystallinity band) and I_{1300} is the integrated area of the group of bands centred at 1300 cm^{-1}. This group of bands at 1300 cm^{-1} is widely accepted as an internal standard for polyethylene.

2.4. Wide angle X-ray scattering

Wide angle X-ray scattering experiments were performed using a Philips equipment with a PW 1710 diffractometer. Radial scans of intensity versus scattering angle (2θ) were recorded in the range 5–40° with identical settings of the instrument by using filtered CuK_α radiation ($\lambda = 1.54$ Å), an operating voltage of 40 kV, and a filament current of 30 mA. In the case of oriented specimens, i.e. isotropic and annealed samples, the beam was applied perpendicular to the straining direction.

The WAXS crystallinity of the isotropic samples was calculated using Eq. 3.

$$\%\chi\text{-WAXS} = \frac{I_c}{(I_c + I_a)}100 \quad (3)$$

where I_c is the integrated area of the crystalline reflections (110) and (200) and I_a is the integrated area of the amorphous halo underneath the crystalline reflections.

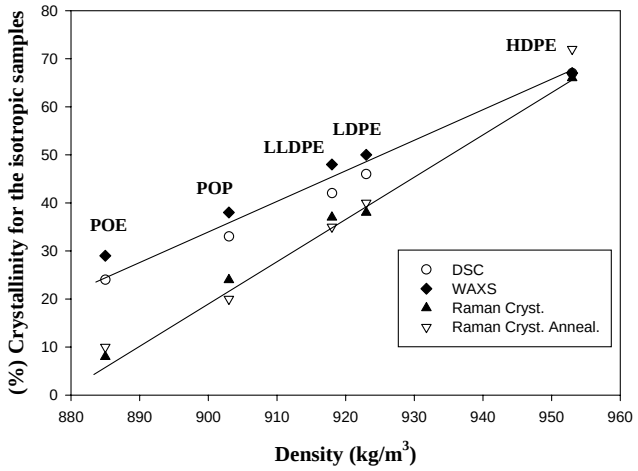

Fig. 3. Crystallinity as determined by Eqs. (1)–(3) as a function of sample density.

2.5. Curve fitting

Raman and WAXS experimental data were processed with the curve-fitting routine in the GRAMS Research 2000 software package (Galactic Industries). Voigt line shapes (convolution of Lorentzian and Gaussian band shapes) and linear baselines were used. Band position and area were derived from the curve-fitting routine. The band position accuracy was estimated to be around $\pm 0.15\ cm^{-1}$. An example of curve-fitting of WAXS and Raman data is shown in Fig. 1.

3. Results and discussion

3.1. Isotropic materials

The melting endotherms and Raman spectra of the isotropic samples are shown in Fig. 2. From Fig. 2(A) it is clear that as sample density decreases (from top to bottom in Fig. 2) the end of melting occurs at lower temperatures. The latter observation does not apply for the LLDPE when compared to LDPE. This is attributed to the LLDPE showing a multiple melting peak endotherm. Multiple melting features are characteristic of LLDPE materials and are caused by the presence of a broad distribution of crystal sizes [3]. This is further attributed to a highly heterogeneous structure that results from non-random incorporation of the comonomer inter-molecularly, and possibly intra-molecularly. Hence, these materials show a melting endotherm—arising from a mixture of crystals with high and low melting point—that extends over a broad range of temperature. The other materials show a single peak melting endotherm that broadens towards lower temperature. This broadening is also attributed to molecular heterogeneity, albeit to a lesser extent than for LLDPE. HDPE shows a sharp melting peak, which suggests a highly homogeneous crystalline phase for this sample.

It is worthy to note that LDPE, LLDPE, POP and POE show a low temperature melting feature at around 40°C. This feature is particularly intense in metallocene-based POE. The presence of this tail is attributed to the annealing-recrystallisation at room temperature of the crystalline fraction with melting point below room temperature [1]. Although the random incorporation of the comonomer in metallocene-based materials is not discussed here, there is a general perception that those commercial grades contain, to some extent, long chain branching. The incorporation of some long chain branching seeks to improve processability issues, e.g. melt strength, etc. Consequently, some degree of molecular heterogeneity is expected in these metallocene materials, which may contribute to the appearance of melting features at very low temperature.

The Raman spectra of the isotropic samples in the range of the internal modes are shown in Fig. 2(B). As sample density decreases, the broad gauche bands (indicated with arrows in Fig. 2(B)) associated with molecular disorder develop, whereas the sharp all-trans bands associated with molecular order tend to vanish. Hence, an overall decrease of the molecular order is observed with decreasing density, as expected. The Raman crystallinity band at $1415\ cm^{-1}$ and the band at $1440\ cm^{-1}$ are also indicated in Fig. 2(B). Both bands are assigned to $-CH_2-$ bending motions and are thought to arise from interchain interaction within the orthorhombic lattice denominated factor group splitting [7] (as is predicted by group theory) or correlation splitting [8]. Thus, a factor group splitting phenomenon, i.e. splitting of one vibrational mode into two components by lattice symmetry effects, is thought to give rise to these bands at 1415 and $1440\ cm^{-1}$. The fact that the separation between the Raman splitting components, 1415 and $1440\ cm^{-1}$ bands, is so high in the Raman spectrum (around $25\ cm^{-1}$) is unusual, and it is thought to be caused by the simultaneous presence of Fermi resonance which enhances the separation. The cited splitting is only observed at room temperature in the $-CH_2-$ bending vibrations (Raman and IR active) and in the $-CH_2-$ rocking modes (only IR active). These two modes are more sensitive to interchain interaction than other vibrational modes because they involve motions predominantly perpendicular to the chain direction. Consequently, the intensity of the band at $1415\ cm^{-1}$ is only associated with ordered chains with orthorhombic lateral order, and therefore it has been extensively used to estimate the orthorhombic crystallinity [6,9,10]. In a recent paper [4], it has been shown that this band can be further used to extract additional information about the nature of the orthorhombic morphology, by means of studying relative changes in position. The relative shift of this band towards the band at $1440\ cm^{-1}$ is interpreted to mean that the interchain interaction in the lattice has decreased, and therefore that the splitting has been weakened to some extent. In our opinion, only two effects can be responsible for a decrease in the

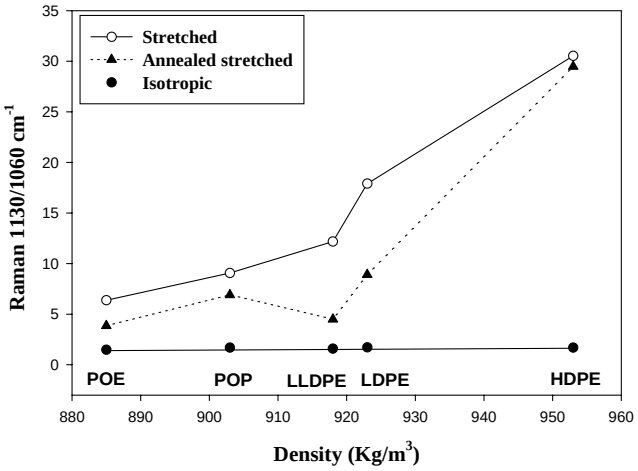

Fig. 4. Raman 1130/1060 cm^{-1} ratio (relative molecular orientation) as a function of sample density.

separation of the components of the splitting: (i) the expansion of the unit cell, i.e. the crystalline density drops; and (ii) the chains loosing the lateral arrangement of the orthorhombic symmetry, i.e. dislocations and other defects. The latter effect is also accompanied by a decrease in crystalline density. From Fig. 2(B), it can be appreciated that the Raman crystallinity band (at 1415cm^{-1}) decreases in intensity with decreasing density, therefore pointing to an orthorhombic crystalline morphology that decreases in content. Changes in the position of this band were also observed as a function of density for the isotropic samples. These are interpreted in terms of changes in crystalline density and will be dealt with later in the paper.

Crystallinity, as calculated by Eqs. (1)–(3), is plotted in Fig. 3 as a function of sample density. The three methods display a linear decrease of crystallinity with decreasing density. A reasonable agreement is seen between the DSC crystallinity Eq. (1) and the WAXS crystallinity Eq. (3), the latter being slightly higher. Distinctly, the Raman crystallinity Eq. (2) shows lower values and the scatter increases with decreasing density. An explanation for this observation is that the samples may have a fraction of crystals with defects (lateral disorder) and a critical drop in crystalline density. This fraction increases in content with decreasing density and is not accounted for in the Raman method. The Raman crystallinity for the annealed isotropic samples is also shown in Fig. 3. This only increases for the annealed HDPE, indicating that the fraction being excluded by Raman crystallinity corresponds to ill-defined crystals with very low crystalline density that cannot be further developed upon annealing due to a high local concentration of branches or/and chain entanglements. Moreover, this fraction could account for the some of the material seen by DSC at very low melting temperature in Fig. 2(A). We are aware that the observations provided here are in disagreement with the standard argument [11] that the Raman crystallinity and the DSC crystallinity yield similar results as they both measure the core crystallinity. This seems to be only in the case of high-density samples. Distinctly, the results shown in Fig. 3 suggest that the Raman crystallinity excludes a fraction of the crystallinity, which most likely has an undeveloped morphology. The fact that the three crystallinities agree well for the HDPE material suggests that this sample contains a robust and homogeneous crystalline morphology made of thick lamella with effective lateral order. Long chain branched materials (LDPE) and bulky short chain branched materials (LLDPE, POP and POE), will however have impediments for the settlement of a robust and continuous crystalline morphology, which in turn will be made of rather smaller and irregular lower density crystals. This is particularly the case of sample POE. This sample is already below the borderline of the density regime under which the morphology changes from lamellar to micellar [1]. Consequently, it is expected to contain a very poorly defined crystalline morphology caused by high random incorporation of a disrupting unit, hexyl branches, throughout the polymer chain.

3.2. Uniaxially stretched and annealed samples

3.2.1. Molecular orientation

Measurements of sample molecular orientation upon uniaxial stretching, and of molecular disorientation upon subsequent annealing were conducted by polarised Raman spectroscopy. Results between different samples can be compared because they all were strained under the same conditions, i.e. until the neck reached two equally spaced marks for all the samples. The annealing temperatures applied (ca. 20°C below the maximum of melting) are summarised in Table 1. Fig. 4 shows the ratio of the area of the Raman band at 1130 to that at 1060 cm^{-1} as a function of sample density. This ratio can be related to the uniaxial molecular orientation of the all-trans segments, to a first approximation within crystals, when $^1I_1$ polarisation conditions are used. Pigeon et al. [12] showed that the ratio of the intensity of these two bands increases (although not linearly) with the increasing of the orientation functions $\langle P2(\cos\theta)\rangle$ and $\langle P4(\cos\theta)\rangle$. The undeformed (isotropic) samples exhibit a similar 1130–1060 cm^{-1} ratio because they have random molecular orientation. In the stretched samples however the relative molecular orientation is seen to decrease with decreasing sample density. This is expected, since crystallinity decreases and chain entanglements are expected to increase with decreasing density. Chain entanglements and other topological constrains impede sample drawability. Crystals are thought to remain oriented after the stress ceases, whereas the amorphous phase is thought to recoil. Accordingly, higher molecular orientation is measured for the samples with higher crystallinity. Upon annealing, the relative molecular orientation of the samples is reduced as they undergo shrinkage. This is particularly the case of LLDPE, LDPE, POP and POE.

HDPE however does not seem to undergo significant reduction of molecular orientation.

Upon stretching the molecular orientation of all-trans segments increases. This is related to the fracture and extension of the crystalline phase but also to extension of tie-molecules and chain entanglements trapped between crystals. By annealing, the samples undergo shrinkage and molecular disorientation of the all-trans segments. This is related to the disorientation of the crystals that melt at temperatures below the annealing temperature and subsequently re-crystallise randomly. In addition, this is also related to recoiling of extended all-trans segments within intercrystalline regions, i.e. tie-molecules, etc., relaxing molecular stress. The molecular disorientation after annealing is higher for LLDPE. This sample shows a broader melting feature (see Fig. 2) and the annealing procedure results in melting–recrystalisation of a larger proportion of the crystalline phase. Further, inter-molecular heterogeneity resulting in potential "molecular segregation" during crystallisation, may be higher for this sample. This allows the low melting point crystal population to re-crystallise randomly after annealing, as this is not molecularly linked to the high melting point oriented crystals. POP and POE are expected to have a random (and higher) incorporation of comonomer. Consequently, the lower crystallinity and an expected highly entangled molecular network prevent the materials from reaching a substantial molecular orientation. These materials do not disorient that much after annealing because re-crystallised crystals are not molecularly segregated. HDPE keeps a fairly constant molecular orientation upon annealing because this sample shows a sharp feature of fusion, well above the annealing temperature and therefore does not undergo substantial melting–recrystallisation during annealing. Further, the likelihood of chain entanglements and tie-molecules trapped between crystals is very low as the branching content is probably very low and the molecular weight is not high.

3.2.2. Crystalline morphology

Figs. 5–7 display the DSC curves, the Raman spectra in the region of the $-CH_2-$ bending (orthorhombic crystallinity region) and the WAXS curves for the, from top to bottom, isotropic, stretched and annealed stretched samples.

3.2.2.1. DSC Fig. 5 shows that upon stretching most of the samples undergo broadening of the melting endotherm towards lower temperature compared to that of the isotropic undeformed samples. This is not the case of the HDPE, which shows a narrower melting peak and at higher temperature. It is known that upon stretching the melting peak of polymers narrows and shifts to higher temperatures [13]. This phenomenon is associated with the molecular orientation of the structure into the straining direction. The latter effect is clearly observed for HDPE in Fig. 5 because this sample shows the highest molecular orientation in Fig. 4. As sample density decreases, the melting feature tends to broaden towards lower temperature and the maximum of melting tends to shift to lower temperature compared to the isotropic samples. These observations are attributed to a decrease in crystal size, and consequently perfection, caused by uniaxial stretching. This structural effect is not seen for HDPE because it is overridden by the cited molecular orientation effect and the disruption of the crystalline phase may be not so severe.

The DSC crystallinity was also measured for the cold drawn and annealed cold drawn materials (see Table 2). This does not substantially change as a result of the different treatments when compared to that of the isotropic samples. However, the changes in the shape of the endotherm described above indicate crystal fractionation upon uniaxial stretching.

Upon annealing of the stretched structures, a melting peak immediately above the annealing temperature is originated. This is the result of the melting–recrystallization of crystals with melting temperatures below the annealing temperature.

The melting tail observed at low temperature (around 40°C, except for HDPE) in the isotropic samples increases relative presence upon stretching. This further decreases relative presence upon annealing, except for sample POE. The presence of this feature at 40°C within those materials indicates that there is a fraction of extremely small/defective crystals with very low melting point, which increases population upon drawing (due to crystal breakage) and decreases again upon annealing (due to crystal regeneration). These low melting point crystals are not able to grow during the annealing process in POE, possibly due to a large content of branches and molecular entanglements impeding crystal development.

3.2.2.2. Raman spectroscopy Fig. 6 shows the Raman spectra in the region of the factor group splitting, i.e. 1400–1520 cm^{-1}, for all the samples. From this figure the development of the two components of the factor group splitting at ca. 1415 cm^{-1} (crystallinity band) and at ca. 1440 cm^{-1}, can be followed through the different treatments and samples. Stretching of the isotropic samples generally results in reduction in intensity and shift in position of the 1415 cm^{-1} band towards higher wavenumber, i.e. towards the band at 1440 cm^{-1}. Upon annealing the band recovers intensity and shifts back towards lower wavenumber. Alterations in intensity, and therefore in Raman crystallinity for the stretched samples, cannot be quantified here because the intensities of the bands are affected by crystalline and amorphous orientation of the samples [4]. However, we can quantify the changes in the separation between the factor group splitting components (separation between the bands at 1415 and at 1440 cm^{-1}). The separation between these bands gives an indication of the health of the orthorhombic crystalline phase after Lagaron et al. [4].

Fig. 8 shows the separation between the components of

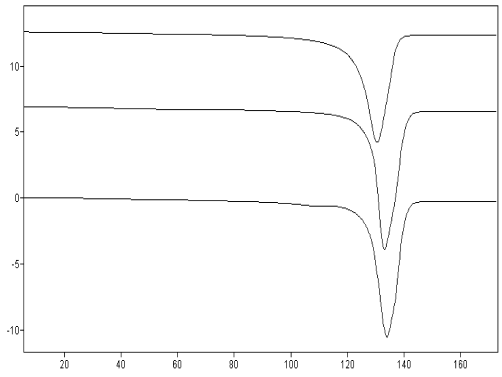

Temperature (ºC)

HDPE

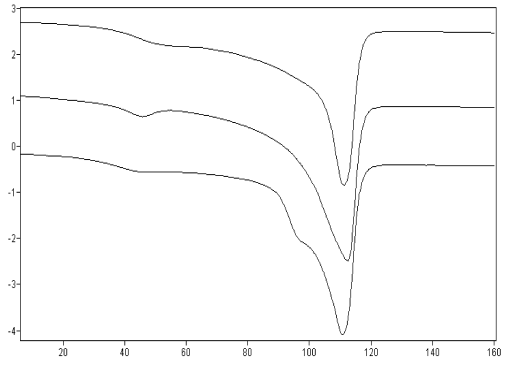

Temperature (ºC)

LDPE

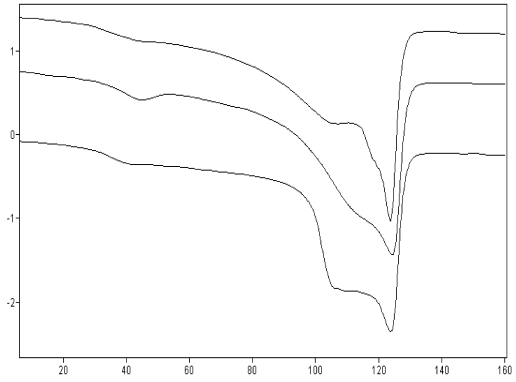

Temperature (ºC)

LLDPE

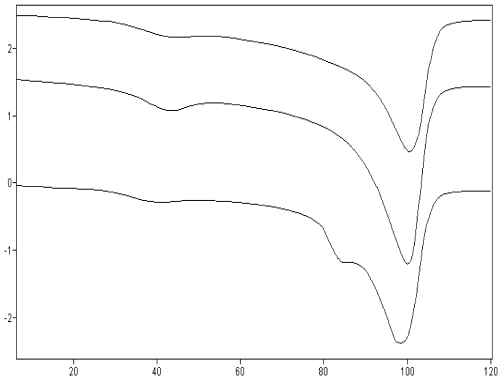

Temperature (ºC)

POP

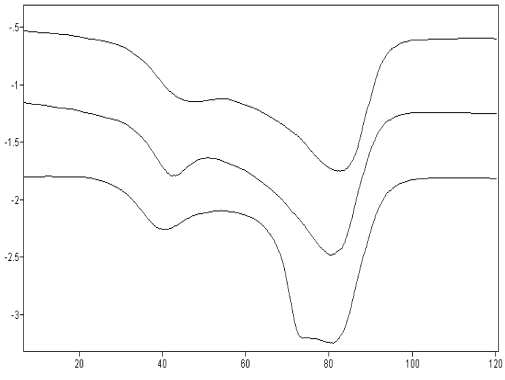

Temperature (ºC)

POE

Fig. 5. DSC melting endotherms of, from top to bottom, isotropic, stretched and annealed stretched samples for all materials.

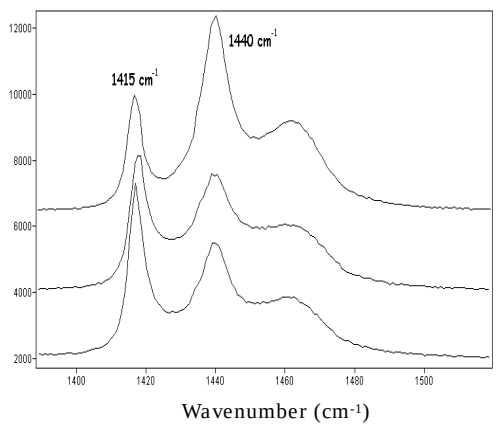

HDPE

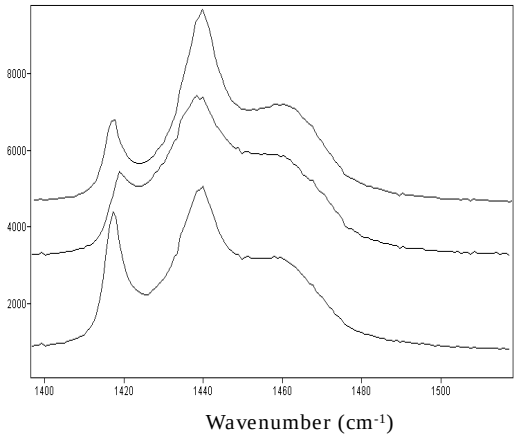

LDPE

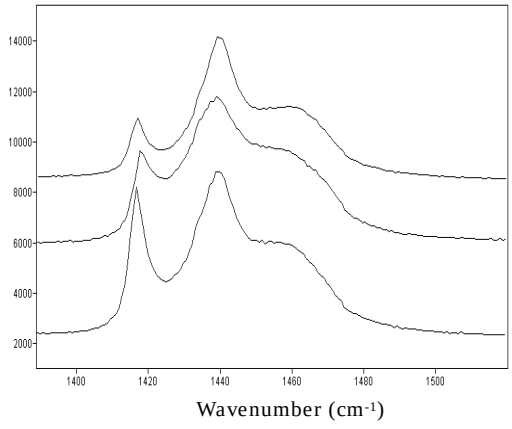

LLDPE

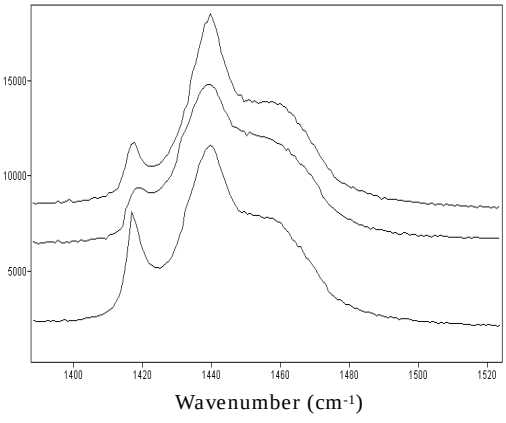

POP

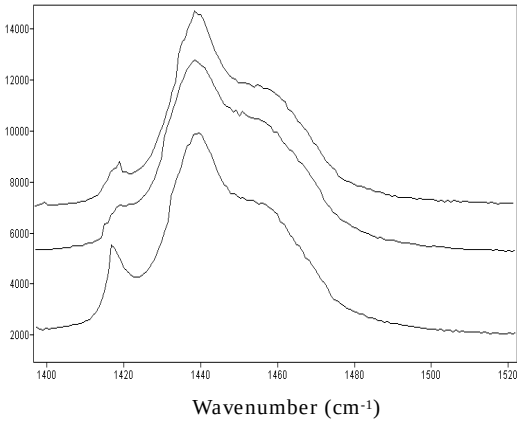

POE

Fig. 6. Raman spectra in the range 1400–1520 cm^{-1} of, from top to bottom, isotropic, stretched and annealed stretched samples for all materials. The spectra are normalised to the intensity of the internal standard band at 1295 cm^{-1}.

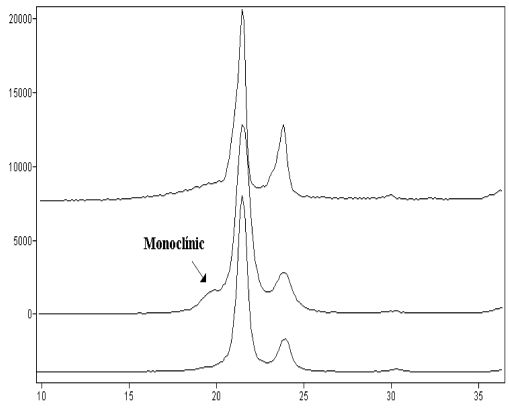

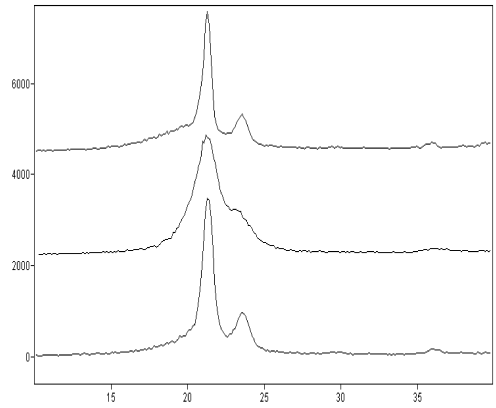

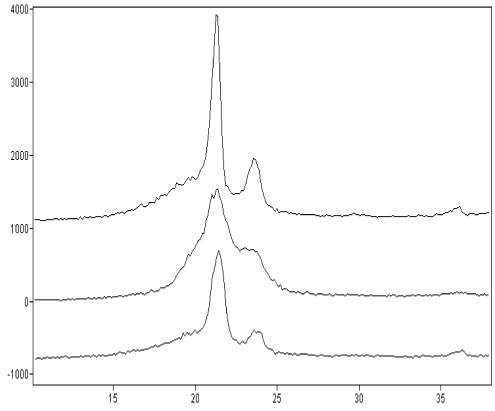

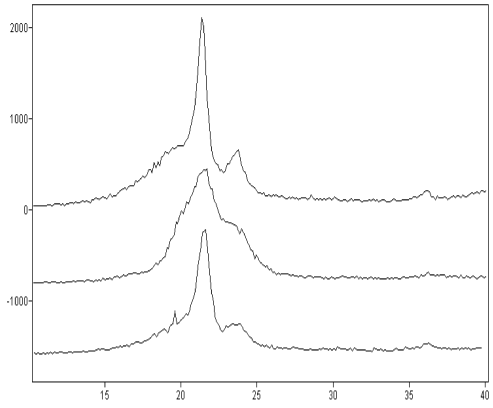

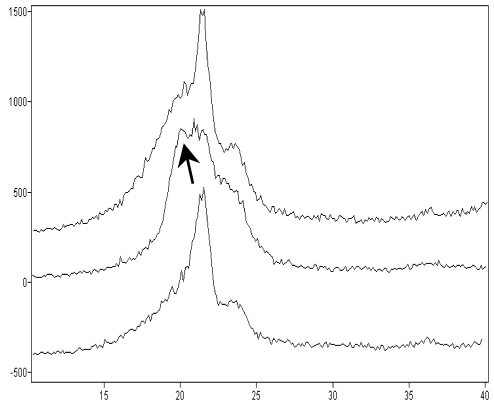

Fig. 7. WAXS curves in the range 10–40° of, from top to bottom, isotropic, stretched and annealed stretched samples for all materials.

the factor group splitting as a function of sample density for isotropic, stretched and annealed stretched samples. This graph also shows the splitting separation of the isotropic samples after annealing. The components of the factor group splitting move towards each other in the stretched samples. This is interpreted as a decrease of the interchain interaction in the lattice caused by the fractionation of the crystalline structure (supported by DSC) upon stretching and the subsequent creation of lateral disorder and lower crystalline density. Expansion of *a* and *b* unit cell parameters has been reported for cold drawn materials [14]. From a recent work [15], this cell expansion increases with increasing draw ratio and, for the same draw ratio, for copolymers. The reduction in splitting seems larger for LDPE in Fig. 8. This is attributed to the long chain branches being pulled through the crystals, resulting in higher damage for the crystalline morphology. In the annealed samples the components of the splitting separate from each other and come close to the splitting separation of the isotropic samples. This is interpreted as a recovery of the health of the orthorhombic crystalline phase towards the perfectness of the isotropic crystals. The fact that the recovery of the factor group splitting is not total for some samples, in particular for the HDPE, may indicate that crystal size is still small after annealing. HDPE does not undergo melting–recrystallisation during annealing, therefore it is possible that the orthorhombic lateral order is recovered but the crystal size (crystalline density) is still small.

From Fig. 8, it can also be seen that the factor group splitting separation in the isotropic samples generally decreases with decreasing sample density. This observation is attributed to the expected decrease in crystalline density, associated with a decrease in crystallinity and melting point [16]. A decrease in crystalline density is partially related to inclusion of some side-chains by some authors (unlikely here for hexyl branches), and is usually associated with defects and reduced lamella thickness. Reduction in lamella thickness (as suggested by a decrease in melting point) in copolymers is thought to cause cell expansion due to surface dilatometric stresses, thermal vibrations and intra-crystalline defects resulting from faster crystallisation at the large undercoolings required. The fact that the cell expansion (crystalline density drop) in polyethylene is mostly due to the enlargement of the *a* cell parameter, the parameter directly responsible for the lateral separation of the two interacting chains within the orthorhombic lattice, explains the marked change in splitting observed for the perpendicular to the chain direction $-CH_2-$ bending vibrational mode in Fig. 8. LLDPE shows a higher splitting value than expected for its density because it has a fraction of crystals with higher melting point (see Fig. 2) and, therefore, higher crystalline density. Upon annealing of the isotropic samples, the splitting value remained practically unchanged as does the crystallinity by Raman in Fig. 3. This is not surprising, since crystal development is largely impeded by branches and molecular entanglements.

3.2.2.3. WAXS Fig. 7 shows the WAXS curves for all the samples. All the materials display the orthorhombic reflections (110) and (200) at angles ca. 21.5 and 24°, respectively. In agreement with the Raman results, the stretched materials show the broadening (smaller crystallite size) and weakening of the orthorhombic patterns, which recover after subsequent annealing. A small peak can be seen at angle 20° in the stretched HDPE. This has been reported before [17] and is usually assigned to a monoclinic (or triclinic) reflection coming from a phase transformation from orthorhombic crystals. This phase transformation is rather small and from an earlier work [4] it is thought to be marginal in stretched HDPEs. Most of the disrupted crystals are therefore ill-defined and small in size orthorhombic crystals. The monoclinic peak is not detected for the other samples either because it is not present or because it is masked by the amorphous halo. The amorphous halo increases in intensity with decreasing density. In stretched POE, it is

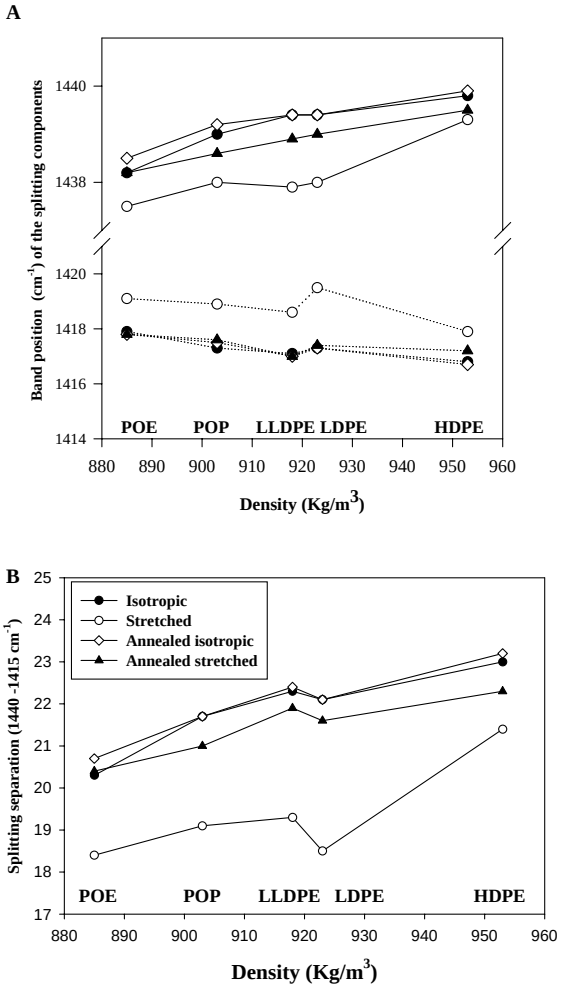

Fig. 8. (A) changes in band position for the components of the factor group splitting and (B) separation between the components of splitting (1440–1415 cm^{-1}) as a function of density for isotropic, stretched, annealed isotropic and annealed stretched samples.

worthy to note (see arrow) that there appears to be a sharp feature at the position where the monoclinic peak is expected. This virtually vanishes in the annealed sample.

4. Conclusions

A comparative study of the crystalline structure of a number of polyethylenes covering a broad range in density and molecular designs has been carried out using Raman, DSC and WAXS. The materials were compared in the isotropic state, after cold drawing, and after annealing of the cold drawn material. Crystallinity for the isotropic samples, as determined by DSC and WAXS, agreed reasonably well and decreased with decreasing density. Crystallinity by Raman was systematically lower and decreased more rapidly with decreasing density. This was attributed to the exclusion by the Raman method of small defective crystals with lateral disorder and a critical drop in crystalline density. Upon cold drawing, the three techniques supported a disruption of the orthorhombic morphology towards a highly ill-defined and fractured crystalline morphology. The orthorhombic crystallinity was further restored upon annealing. The separation of the components of the $-CH_2-$ bending factor group splitting phenomenon, which gives rise to the Raman orthorhombic crystallinity band, generally decreased with decreasing density. This spectroscopic phenomenon was confirmed to be strongly sensitive to changes in crystalline density and lattice lateral order. The relative molecular orientation, as measured by Raman, increased with increasing density and was attributed to orientation of the all-trans segments, which are placed mainly within crystals. Upon annealing, the samples underwent shrinkage and molecular disorientation, except the HDPE. The molecular disorientation is attributed to the melting and subsequent random re-crystallisation of the low melting point crystalline fraction of the materials. This can also be attributed to recoiling of tie-molecules and molecular entanglements trapped between crystals.

Acknowledgements

This research was funded by the MINER/Spain (programme ATICA) and the Agency of Economic Development (ADE) of Castilla y León/ Spain.

References

[1] Bensason S, Minick J, Moet A, Chum S, Hiltner A, Baer E. J Appl Polym Sci, Part B Polym Phys 1996;34:1301.
[2] Mathot VBF, Scherremberg RL, Pijpers TFJ, Bras W. J Thermal Anal 1996;46(3–4):681.
[3] Wilfong DL, Knight GW. J Appl Polym Sci, Polym Phys 1990;28:861.
[4] Lagaron JM, Dixon NM, Reed W, Pastor JM, Kip BJ. Polymer 1999;40:2569.
[5] Rodriguez-Cabello JC, Martin-Monge J, Lagaron JM, Pastor JM. Macromol Chem Phys 1998;199:2767.
[6] Strobl GR, Hagedorn W. J Polym Sci, Polym Phys Ed 1978;16:1181.
[7] Ishii K, Nukaga M, Hibino Y, Hagiwara S, Nakayama H. Bull Chem Soc Jpn 1995;68:1323.
[8] Bower DI, Maddams WF. The vibrational spectroscopy of polymers. Cambridge: Cambridge University Press, 1989.
[9] Gloting M, Mandelkern L. Colloid Polym Sci 1982;260:182.
[10] Gloting M, Domszy R, Mandelkern L. J Polym Sci, Polym Phys Ed 1983;21:285.
[11] L. Mandelkern et al. Physical properties of polymers. ACS Professional Reference Book, 1993.
[12] Pigeon M, Prud'homme RE, Pezolet M. Macromolecules 1991;24:5687.
[13] Bershtein VA, Egorov VM. Differential scanning calorimetry of polymers. Chichester: Ellis Horwood, 1994.
[14] Glenz W, Peterling A, Wilke W. J Polym Sci 1971;9:1243.
[15] M.E. Vickers. Polymer'98. Brighton, UK, 1998, p. 328.
[16] Howard PR, Crist B. J Polym Sci Phys 1989;27:2269.
[17] Vickers ME, Fischer H. Polymer 1995;36:2667.